J. Earth Syst. Sci. (2019) 128:116
https://doi.org/10.1007/s12040-019-1102-0

Petrology and geochemistry of mafic dyke and sills in Cumbum Formation, of the Proterozoic Nallamalai fold belt, Rajampet area, Andhra Pradesh, India

Sankha Das* and Munmun Chakraborty

Geological Survey of India, SU: Andra Pradesh and Telangana, Southern Region, Hyderabad, India.
**Corresponding author. e-mail: sankhad56@gmail.com*

MS received 28 March 2018; revised 26 July 2018; accepted 27 July 2018; published online 8 May 2019

Intensely deformed Proterozoic Nallamalai fold belt (NFB) occupies the eastern part of undeformed, Proterozoic Cuddapah basin and is separated from Cuddapah basin by easterly dipping Rudravaram thrust line. Igneous activity in NFB is represented by intrusive syenite and lamproite dykes. This study brings out the petrological and geochemical character of unreported intrusive dolerite dykes and sills within the Cumbum Formation of NFB. The dykes are undeformed, whereas the sills suffered D1 phase of deformation, although both are petrologically and geochemically similar. The rocks are highly fractionated sub-alkaline tholeiite, consist mainly of clino-pyroxene and plagioclase. Chondrite-normalised rare earth element (REE) plot shows enriched light rare earth element (LREE) and flat heavy rare earth element (HREE). A primitive mantle-normalised multi-element spider diagram shows troughs in Nb, Ta, Ti and Zr indicating subduction zone character. Tectonic discrimination plots indicate both within-plate and subduction zone environment of formation. Geochemical modelling also indicates enriched spinel peridotite as a probable source for dykes and sills. We suggest that the lithospheric mantle beneath NFB got enriched by subduction-derived fluid around 1.6 Ga, and in later stage, these dykes and sills were generated by extension of the enriched lithosphere at different phases in turn inheriting the subduction zone geochemical characters.

Keywords. Nallamalai fold belt; Cumbum Formation; mafic dyke and sills.

1. Introduction

Variably oriented dyke swarms are common features of the Archaean cratons in India (Srivastava and Singh 2004). Study of Archaean/Proterozoic mafic dykes is important to understand the geodynamic processes and mantle condition prevailing at that time. The general trend of dykes in and around Cuddapah basin is NE–SW, although some N–S and E–W trending dykes are also present (Srivastava *et al.* 2014). French *et al.* (2008) have done a detailed analysis of the dykes of Bastar and Dharwar cratons (Cuddapah basin). Majority of the dykes from the Bastar and Cuddapah basins show age around 1.9 Ga, and this resemblance in age has been postulated as a result of widespread extensional tectonics around 1.9 Ga resulting in mafic/ultramafic magmatism in the southeastern part of Dharwar protocontinent and has been informally called as *Bastar–Cuddapah Large Igneous Province.* Such type of mafic/ultramafic magmatism around 1.9 Ga is also found in Superior craton and Kalahari craton of Africa. This widespread synchronous magmatism

in Bastar–Cuddapah–Superior and Kalahari cratons has been linked to the existence of the oldest supercontinent/craton Ur (French *et al.* 2008). Study of these dyke swarms provides an understanding and record of the large igneous provinces (LIPs), which might help in palaeo-tectonic reconstructions by precise geo-chronological and geomagnetic dating (Srivastava *et al.* 2014). LIPs represented by giant dyke swarms, sill provinces and layered intrusions are examples of deep-seated plumbing systems, which might help in locating ancient plumes and in turn locating breakup centres of ancient supercontinent (Srivastava 2011). Halls (1982) has dealt in detail regarding the importance of study of dyke swarms and has opined that though dyke swarms often represent monotonous lithology, their study may bring out the details of Archaean craton assembly and the stress pattern prevailing at the time of intrusion in the area. Study of dyke swarms can eventually lead to identification of mantle plumes (Halls 1982). This paper brings out the petrology and geochemistry of unreported dolerite dyke and sills, intrusive within the sediments of Cumbum Formation of Nallamalai fold belt (NFB) and its significance with respect to the adjoining terrains and evolution of NFB.

2. Geological setting

Undeformed Cuddapah basin (figure 1) represents a classic example of intra-cratonic sedimentary basin. King (1872) carried out pioneering geological work in the Cuddapah basin and recorded his observations in his classic memoir 'On the Kadapah–Kurnool Formations in the Madras Presidency'. King suggested that the Kadapah and Kurnool are possibly of Palaeozoic age and have been deposited over crystalline basement. He subdivided the rocks of Cuddapah 'System' into four 'series', viz., Papaghni, Cheyair, Nallamalai and Krishna, in ascending order. He named the rocks occurring around Pullampet–Rajampet area under Pullampet 'stage' of the Cheyair 'Series' of the Cuddapah 'System' and described shale, slate, quartzite, limestone and dolomite. For the first time, he identified the presence of acid volcanic (quartzofeldspathic) rocks in the Tadpatri shale which is considered to be time equivalent of the lithounits of the Pullampet Formation. Nagaraja Rao *et al.* (1987) recognised four sub-basins within the Cuddapah basin, namely Papaghni, Kurnool, Srisailam and the Palnad sub-basins. The Cuddapah supergroup is divided into three groups, Papaghni, Chitravati and Nallamalai from bottom to top (table 1). The relatively undeformed Cuddapah basin is overlain by intensely deformed and folded NFB.

The NFB consists of intensely deformed rocks belonging to the Nallamalai group. The Nallamalai group comprises quartzites (Bairenkonda/Nagari Formation) overlain by argillaceous sediments with bands of dolomite and quartzite (Pullampet/Cumbum Formation). In the east central part

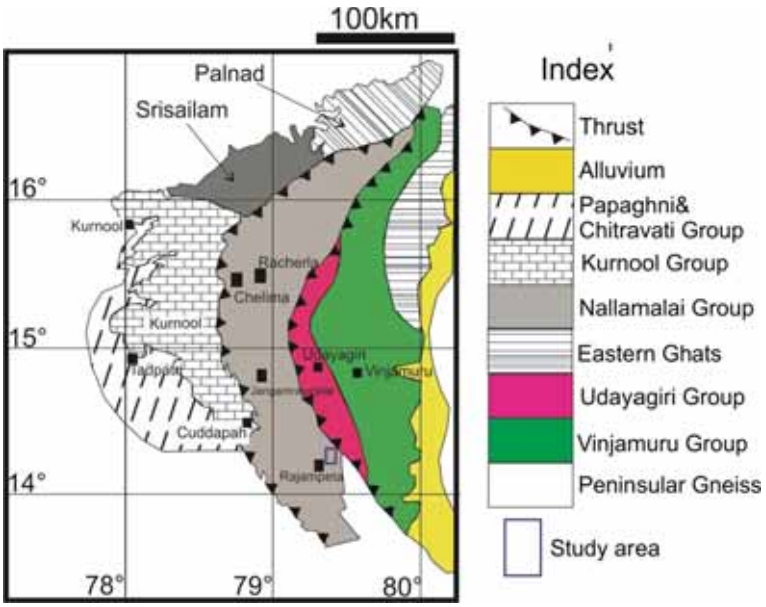

Figure 1. Generalised geological map of the Cuddapah basin and Nellore Schist belt showing study area.

Table 1. *Stratigraphy of Cuddapah supergroup.*

Group	Formation	Thickness (m)	Lithology	Age of intrusive
Kurnool group	Nandyal shale	50 ± 100	Shale	
	Koilkuntla limestone	15 ± 50	Limestone	
	Paniam quartzite	10 ± 35	Quartzite	
	Owk shale	10 ± 15	Shale-ocherous	
	Narji limestone	100 ± 200	Limestone	
	Banaganapalli quartzite	10 ± 50	Conglomerate, quartzite	
.....	Unconformity	.....	.....	.....
	Srisailam quartzite	300	Quartzites and shale	
.....	Unconformity	.....	.....	.....
Nallamalai group	Cumbum: phyllite, slate, quartzite, dolomite			
	Cumbum (Pullampet) Formation	2000	Pullampet: shale, dolomite, quartzite	Racherla syenite: 1326 ± 73 Ma, Chelima lamproite: 1328 ± 52 Ma, Zangamrajupalle lamproite: 1090 Ma
	Bairenkonda (Nagari) quartzites	1500 ± 4000	Bairenkonda: quartzite and shale Nagari: conglomerate, quartzites and shales with intrusives	
.....	Angular unconformity	.....	.....	.....
Chitravati group	Gandikota quartzite	300	Quartzites and shale	
	Tadpatri Formation	4600	Shale, ash fall tuffs, quartzite, dolomite with intrusives	Mafic sill: 1899 ± 20 Ma
	Pulivendla quartzite	1 ± 75	Conglomerates and quartzite	
.....	Disconformity	.....	.....	.....
Papaghni group	Vempalli Formation	1900	Stromatolitic dolomite, dolomite mudstone, chert breccia and quartzite with basic flows and intrusives	
	Gulcheru quartzites	28 ± 210	Conglomerate arkose, quartzite and shale	
			Non-conformity	
.....	Archaean and Dharwar	.....	.....	.....

of the NFB, both the Bairenkonda Formation and Cumbum Formation have been divided (Saha and Tripathy 2012) into three members, viz., Bairenkonda quartzite consisting of Tekurupeta quartz-phyllite member, Porumamilla quartzite member and Kalavakunta member and Cumbum Formation consisting of Chintalapalle slate member, Sonam Cherevu phyllite member and Pandurangapuram quartzite member, from bottom to top. NFB is separated from the undeformed Cuddapah basin along east dipping Rudravaram thrust line. The eastern boundary of NFB is separated from Nellore Schist belt (NSB), along east dipping Velikonda Thrust Front. NFB is further divided into four different subbasins from south to north, viz., Pullampet/Rajampet, Zangamrajupalle, Markapur and Agnigundla.

Stratigraphically, NSB (located at the eastern part of NFB) is divided into a western Udayagiri group and eastern Vinjamuru group (Ramam and Murty 1997). Dobmeier and Raith (2003) have

divided NSB into eastern Vinjamuru domain and western Udayagiri domain. However, subsequently, NSB has been divided into four tectonic units, viz., the Vinjamuru group, the Kandra complex, the Kanigiri complex and the Udayagiri group from older to younger. The Udayagiri group is dominated by green schist facies metasediments with local intra-formational oligomictic quartz-pebble conglomerates. The Vinjamuru group is dominated by metabasic volcanics metamorphosed in amphibolite facies intercalated with psammo-pelitic schist, quartzites, gneisses and migmatites and locally abundant felsic metavolcanics, marbles, calc-silicate gneisses and kyanite schist

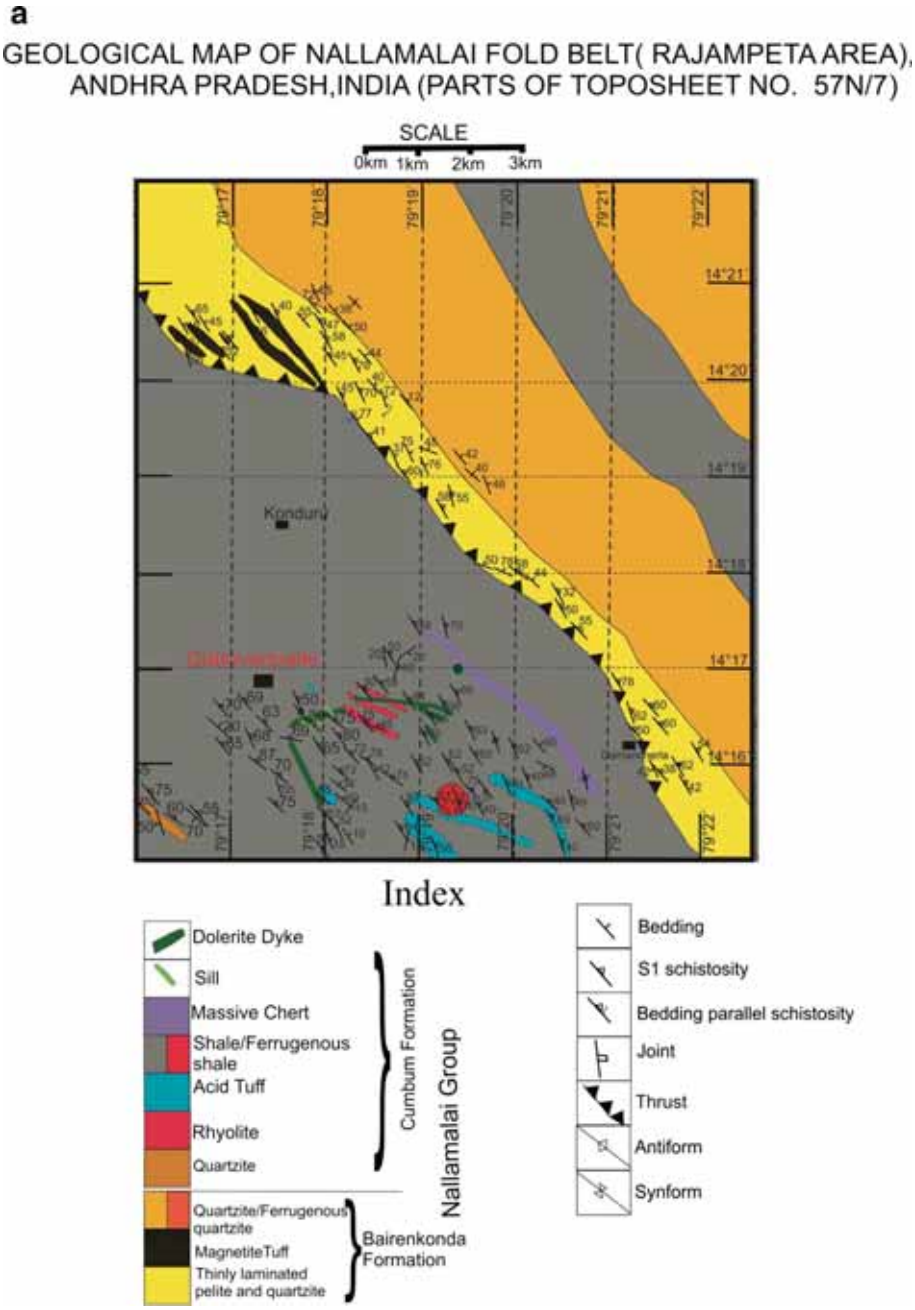

Figure 2. (**a**) Detailed geological map of the study area, (**b**) dyke cross-cutting the shale of Cumbum Formation of Nallamalai group, (**c**) mafic sill intruded parallel to the regional foliation (S1) of the shale of Cumbum Formation, (**d**) photomicrograph of chlorite formed due to alteration of pyroxene, (**e**) photomicrograph of ophitic texture in dyke, (**f**) photomicrograph of inter-granular texture in a dyke, (**g**) photomicrograph of unaltered Cpx in dyke, (**h**) photomicrograph of chlorite formed due to alteration of pyroxene in sill. Note the development of S–C fabric showing dextral sense of shearing, (**i**) photomicrograph of C′ type of shear band in a sill showing dextral sense of shearing and (**j**) pyroxene thermometry after Lindsley (1983).

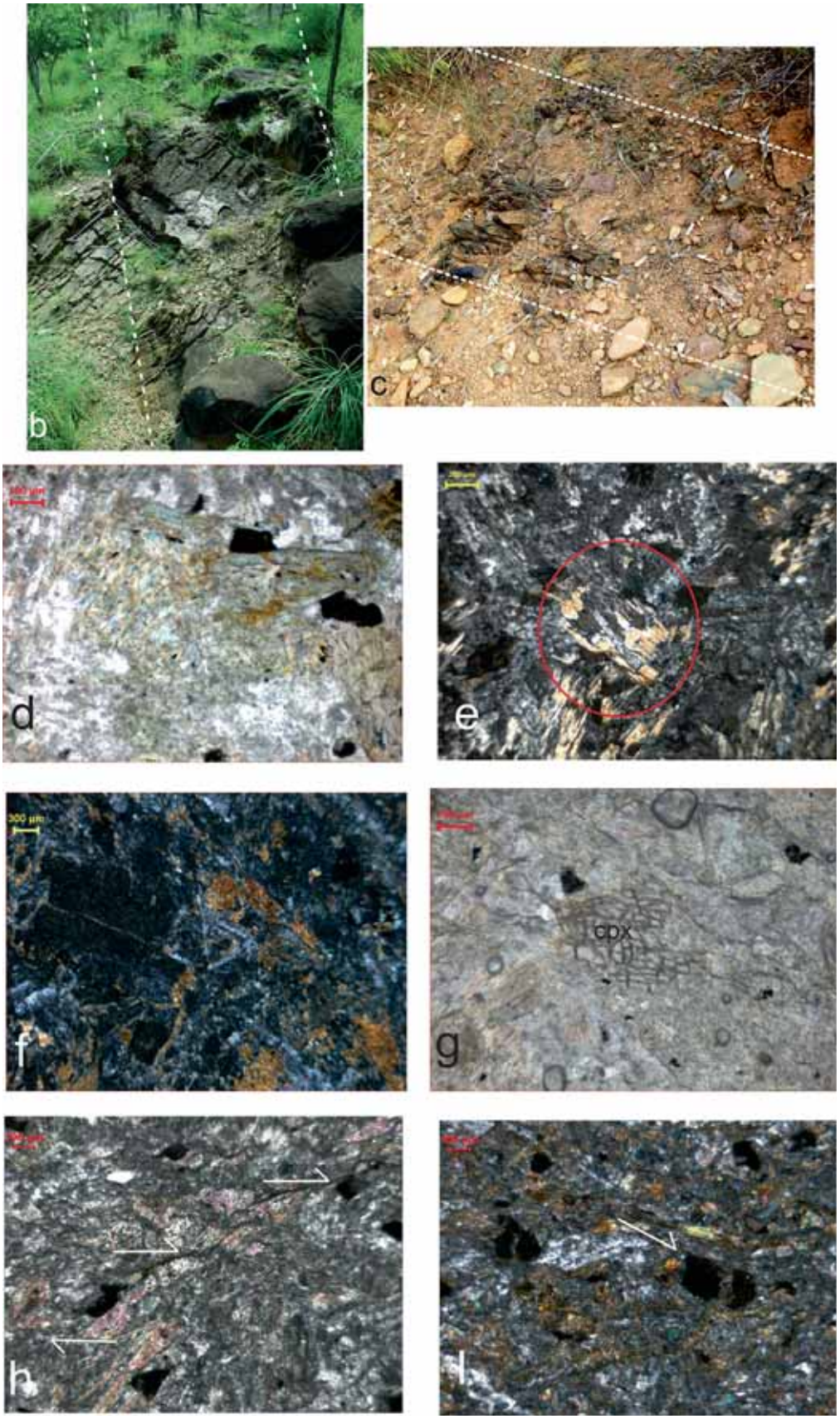

Figure 2. (*Continued.*)

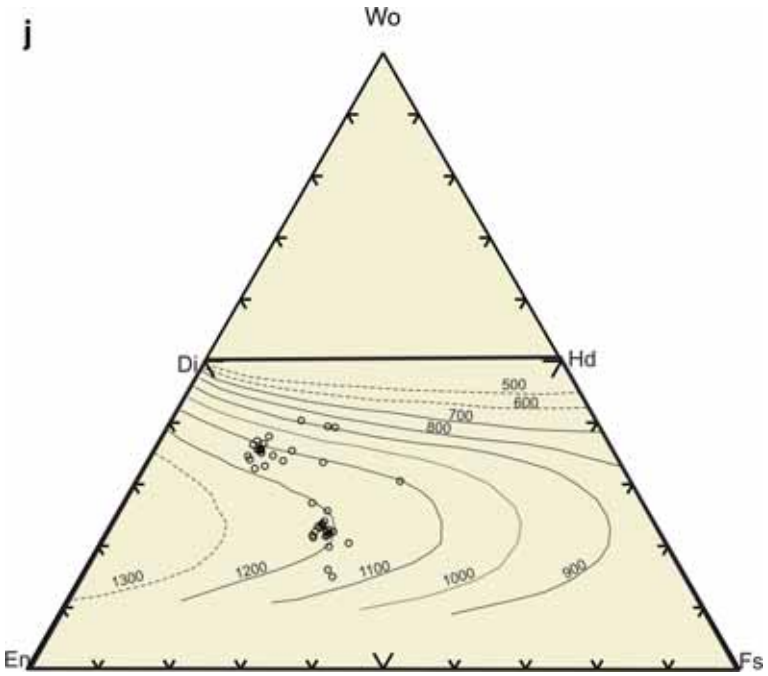

Figure 2. (*Continued.*)

(Vasudevan and Rao 1975; Narayana Rao 1983; Ramam and Murty 1997). Metabasalt of Vinjamuru group (from Chaganam and Chundi) is dated at 2654 ± 100 Ma by Sm–Nd systematic (Ravikant 2010). The Kandra ophiolitic complex (KOC) is located at the southernmost margin of the NSB formed in a continental back arc basin setting around 1.85 Ga (Saha and Sain 2018). Kanigiri ophiolitic mélange (KOM) is located near the central part of the NSB, sandwiched between Udayagiri and Vinjamuru groups. Plagiogranite and gabbro from this ophiolitic mélange has been dated back to 1330 Ma (Vijaya Kumar *et al.* 2006; Dharma Rao *et al.* 2009; Saha and Sain 2018). KOC is considered as supra-subduction zone ophiolite with back-arc affinity, whereas KOM is considered as supra-subduction zone ophiolite with oceanic arc affinity (Saha and Sain 2018). As KOC formed at around 1.9 Ga and KOM at around 1.3 Ga, two episodes of plate convergences away from the eastern margin of eastern Dharwar Craton (EDC) has been suggested by Saha and Sain (2018) separated by an age gap of nearly 600 Ma. First, the KOC formed around 1.9 Ga as a back-arc basin due to an eastward subduction. Later on, during 1.6 Ga Vinjamuru group, volcanics were generated due to a westward subduction (refer figure 11 of Saha and Sain 2018) in an intra-oceanic island arc setting and KOM formed around 1.3 Ga due to another back-arc basin opening and its partial closure (Saha and Sain 2018). Based on geochemistry, Das and Shukla (2016) have suggested that the Vinjamuru domain metabasalts were generated in an island arc setting. NFB was generated at the outer part of this orogeny, and both NSB and NFB have been considered as part of the same island arc archipelago (Saha and Sain 2018). Later during 0.78 Ga (Rodinia breakup), the whole package consisting of NSB and NFB coalesced with the eastern margin of Cuddapah basin.

Igneous activity in Cuddapah basin is confined to the lower part of the Cuddapah supergroup. Vempalle Formation mainly consists of vesicular basaltic lava flows (Anand *et al.* 2003). The thickest (∼50 m) lava flows are recorded at Pulivendla, Vempalle and Animala. Lavas and sills of Vempalle Formation consist of albitic feldspar and augite variety of clino-pyroxene, along with chlorite, white mica and iron oxides. The Tadpatri Formation is intruded by numerous mafic and ultramafic sills, which are exposed at different stratigraphic levels. The thickest sill (∼200 m) is highly differentiated and extends for 150 km length. Tadpatri sills are relatively unaltered in nature, consists of olivine, pyroxene, phlogopite and some spinel. The lower part of the sills shows cumulate texture with fresh olivine, while the upper part of

Table 2. *EPMA analysis result of dolerite dyke (all values in weight percentage).*

Sample no.	18RJM	18RJM	18RJM	18RJM	18RJM	149RJM	149RJM
Rock type							
Phase	Cpx	Cpx	Cpx	Cpx	Cpx	Cpx	**Cpx**
Sample point	16/1	19/1	21/1	22/1	31/1	45/1	51/1
SiO_2	54.598	52.927	53.523	57.375	51.839	49.131	52.967
TiO_2	0.148	0.433	0.017	1.854	0.056	0.009	0.01
Al_2O_3	1.415	2.164	0.852	1.352	2.466	3.709	1.093
Cr_2O_3	0.109	0.000	0.064	0.006	0.073	0.045	0.000
FeO	16.262	15.94	15.83	13.08	17.108	17.549	15.997
MnO	0.237	0.228	0.22	0.211	0.299	0.255	0.191
MgO	13.544	12.988	13.636	12.196	12.126	13.654	14.023
CaO	12.428	12.043	12.64	12.457	12.59	10.653	12.665
Na_2O	0.185	0.339	0.085	0.161	0.305	0.11	0.166
K_2O	0.047	0.125	0.011	0.081	0.104	0.02	0.028
NiO	0.008	0.000	0.097	0.000	0.000	0.000	0.000
Total	**98.914**	**97.084**	**97.003**	**98.733**	**96.991**	**97.115**	**97.078**
Si	2.055	2.031	2.056	2.116	2.012	1.971	2.037
Ti	0.004	0.012	0.000	0.051	0.002	0.000	0.000
Al	0.063	0.098	0.039	0.059	0.113	0.168	0.049
Cr	0.003	0.000	0.002	0.000	0.002	0.001	0.000
Fe	0.510	0.510	0.507	0.402	0.553	0.564	0.513
Mn	0.008	0.007	0.007	0.007	0.010	0.008	0.006
Mg	0.765	0.748	0.786	0.675	0.706	0.789	0.809
Ca	0.501	0.495	0.520	0.492	0.523	0.440	0.522
Na	0.013	0.025	0.006	0.011	0.023	0.008	0.012
K	0.002	0.006	0.001	0.004	0.005	0.001	0.001
Ni	0.000	0.000	0.003	0.000	0.000	0.000	0.000

Sample no.	149RJM	149RJM	149RJM	149RJM	149RJM	149RJM	149RJM	149RJM	149RJM
Rock type									
Phase	Plag	Plag	Plag	Plag	Plag	Plag	Plag	Plag	Plag
Sample point	37/1	38/1	39/1	41/1	48/1	50/1	53/1	54/1	55/1
SiO_2	67.412	67.068	66.778	65.821	66.85	65.206	66.581	65.442	66.477
TiO_2	0.000	0.000	0.018	0.006	0.002	0.000	0.000	0.000	0.000
Al_2O_3	20.404	19.366	19.716	19.812	19.725	19.307	18.962	19.392	20.772
Cr_2O_3	0.000	0.000	0.000	0.000	0.005	0.02	0.000	0.004	0.001
FeO	0.078	0.147	0.000	0.161	0.261	0.069	0.314	0.097	0.125
MnO	0.047	0.046	0.000	0.000	0.023	0.000	0.001	0.026	0.027
MgO	0.037	0.059	0.000	0.016	0.119	0.014	0.102	0.000	0.035
CaO	0.144	0.261	0.112	0.266	0.143	0.179	0.103	0.156	0.144
Na_2O	11.547	11.605	6.927	10.983	9.117	11.915	11.237	9.41	11.525
K_2O	0.094	0.288	4.486	0.173	0.844	0.101	0.564	1.87	0.114
NiO	0.011	0.000	0.000	0.000	0.000	0.001	0.000	0.000	0.000
Total	**99.733**	**98.794**	**97.951**	**97.197**	**98.048**	**98.709**	**98.791**	**98.348**	**99.185**
Si	3.0518	3.0748	3.0845	3.0545	3.0887	3.0819	3.0950	3.0922	3.0301
Ti	0.000	0.000	0.001	0.000	0.000	0.000	0.000	0.000	0.000
Al	1.087	1.045	1.071	1.082	1.056	1.042	1.022	1.046	1.114
Cr	0.000	− 0.001	0.000	0.000	0.000	0.001	0.000	0.000	0.000
Fe	0.003	0.006	0.000	0.006	0.010	0.003	0.012	0.004	0.005
Mn	0.002	0.002	0.000	0.000	0.001	0.000	0.000	0.001	0.001
Mg	0.003	0.004	0.000	0.001	0.008	0.001	0.007	0.000	0.002
Ca	0.007	0.013	0.006	0.013	0.007	0.009	0.005	0.008	0.007
Na	1.012	1.030	0.619	0.986	0.803	1.058	0.996	0.835	1.017
K	0.005	0.017	0.265	0.010	0.049	0.006	0.033	0.109	0.007
Ni	0.000	0.000	0.000	0.000	0.000	0.000	0.000	0.000	0.000

Table 2. *(Continued.)*

Sample no.	12RJM	12RJM	12RJM	12RJM	12RJM	12RJM	12RJM	12RJM	12RJM	12RJM	12RJM	12RJM
Rock type												
Phase	Cpx	Cpx	Cpx	Cpx	Cpx	Cpx	Cpx	Cpx	Cpx	Cpx	Cpx	Cpx
Sample point	56/1	57/1	58/1	59/1	60/1	61/1	62/1	63/1	64/1	65/1	66/1	68/1
SiO_2	49.65	53.845	51.035	49.888	50.525	51.157	48.643	53.002	50.605	50.36	51.994	51.601
TiO_2	0.56	0.094	0.695	0.603	0.684	0.476	0.937	0.409	0.593	0.557	0.48	0.345
Al_2O_3	1.969	1.586	1.914	2.386	1.888	1.991	1.774	2.62	2.415	2.247	2.033	1.453
Cr_2O_3	0.2	0.005	0.048	0.429	0.048	0.401	0.000	0.000	0.41	0.533	0.405	0.054
FeO	10.293	15.164	10.718	8.777	11.818	8.213	14.815	14.764	8.908	8.242	8.431	11.191
MnO	0.248	0.235	0.218	0.242	0.205	0.203	0.332	0.222	0.204	0.225	0.183	0.206
MgO	17.112	13.02	16.585	16.245	15.15	16.827	13.805	14.335	16.035	16.254	17.604	14.003
CaO	17.605	12.893	17.84	19.349	18.41	19.427	17.128	13.205	19.485	20.178	18.491	19.939
Na_2O	0.242	0.681	0.205	0.242	0.222	0.186	0.231	0.09	0.256	0.215	0.255	0.205
K_2O	0.036	0.368	0.001	0.011	0.004	0.000	0.029	0.04	0.005	0.038	0.000	0.004
NiO	0.019	0.077	0.115	0.043	0.000	0.000	0.000	0.016	0.045	0.08	0.009	0.000
Total	**97.934**	**97.967**	**99.373**	**98.216**	**98.934**	**98.799**	**97.636**	**98.666**	**98.961**	**98.93**	**99.868**	**98.936**
Si	2.039	2.171	2.055	1.892	1.918	1.917	1.901	1.995	1.903	1.896	1.922	1.956
Ti	0.017	0.003	0.021	0.017	0.019	0.013	0.027	0.012	0.017	0.016	0.013	0.010
Al	0.095	0.075	0.091	0.106	0.084	0.088	0.082	0.116	0.107	0.100	0.088	0.065
Cr	0.006	0.000	0.002	0.013	0.001	0.012	0.000	0.000	0.012	0.016	0.012	0.002
Fe	0.352	0.510	0.360	0.277	0.374	0.256	0.482	0.463	0.279	0.259	0.260	0.354
Mn	0.009	0.008	0.007	0.008	0.007	0.006	0.011	0.007	0.006	0.007	0.006	0.007
Mg	0.594	0.444	0.564	0.924	0.863	0.946	0.809	0.809	0.905	0.918	0.976	0.796
Ca	0.775	0.557	0.770	0.786	0.749	0.780	0.717	0.533	0.785	0.814	0.732	0.810
Na	0.019	0.053	0.016	0.018	0.016	0.013	0.017	0.007	0.019	0.016	0.018	0.015
K	0.002	0.019	0.000	0.001	0.000	0.000	0.001	0.002	0.000	0.002	0.000	0.000
Ni	0.001	0.002	0.004	0.001	0.000	0.002	0.000	0.000	0.001	0.002	0.000	0.000

Sample no.	12RJM	12RJM	12RJM	12RJM	12RJM	12RJM	12RJM	12RJM	12RJM
Rock type									
Phase	Cpx	Cpx	Cpx	Cpx	Cpx	Cpx	Cpx	Cpx	Cpx
Data set/point	69/1	71/1	72/1	74/1	75/1	76/1	77/1	78/1	80/1
SiO_2	49.553	50.184	50.26	50.107	50.493	51.014	50.909	50.17	49.121
TiO_2	0.72	0.607	0.685	0.654	0.56	0.544	0.437	0.453	0.635
Al_2O_3	2.637	1.987	2.148	2.495	2.409	2.842	1.69	1.916	1.719
Cr_2O_3	0.495	0.08	0.256	0.394	0.398	0.635	0.378	0.249	0.021
FeO	8.561	10.411	10.151	9.128	8.934	8.937	9.694	8.994	11.591
MnO	0.239	0.296	0.212	0.216	0.185	0.227	0.146	0.288	0.231
MgO	16.279	16.132	16.672	16.318	16.438	16.16	17.687	15.525	15.91
CaO	19.441	18.453	17.49	18.727	19.121	18.262	17.785	19.828	17.834
Na_2O	0.291	0.259	0.215	0.232	0.215	0.282	0.231	0.236	0.193
K_2O	0.000	0.03	0.019	0.013	0.026	0.029	0.000	0.038	0.000
NiO	0.000	0.000	0.038	0.000	0.019	0.000	0.054	0.061	0.000
Total	**98.146**	**98.433**	**98.146**	**98.272**	**98.797**	**98.901**	**98.992**	**97.757**	**97.185**
Si	1.881	1.907	1.907	1.897	1.900	1.911	1.911	1.916	1.900
Ti	0.020	0.017	0.019	0.019	0.016	0.015	0.012	0.013	0.018
Al	0.118	0.089	0.096	0.111	0.107	0.125	0.075	0.086	0.078
Cr	0.015	0.002	0.008	0.012	0.012	0.019	0.011	0.008	0.001
Fe	0.271	0.330	0.321	0.288	0.280	0.279	0.303	0.286	0.374
Mn	0.008	0.010	0.007	0.007	0.006	0.007	0.005	0.009	0.008
Mg	0.927	0.919	0.949	0.927	0.928	0.908	0.996	0.889	0.923
Ca	0.790	0.751	0.711	0.760	0.771	0.733	0.715	0.811	0.739
Na	0.021	0.019	0.016	0.017	0.016	0.020	0.017	0.017	0.014
K	0.000	0.001	0.001	0.001	0.001	0.001	0.000	0.002	0.000
Ni	0.000	0.000	0.001	0.000	0.001	0.000	0.002	0.002	0.000

Table 3. *Standards used for major oxide (%) and trace elements (ppm) for XRF machine.*

Sl. no.	1	2	3	4	5	6	7	8	9	10	11	12
Standard	NIM-S	GSR-2	JSL-1	GSR-5	JA-2	GSR-7	SARM-50	NIM-P	JB-3	JGb-2	GSI-SA-1	GSR-3
SiO_2	63.63	60.62	59.35	59.23	56.18	54.48	51.56	51.1	51.04	46.68	44.99	44.64
Al_2O_3	17.34	16.17	17.62	18.82	15.32	17.72	15.28	4.18	16.89	23.32	30.05	13.83
Fe_2O_3	1.4	4.9	6.84	7.6	6.14	7.41	11	12.7	11.88	6.85	2.87	13.4
MnO	0.01	0.08	0.062	0.02	0.11	0.12	0.17	0.22	0.16	0.13	0.039	0.17
MgO	0.46	1.72	2.48	2.01	7.68	0.65	7.57	25.33	5.2	6.24	2.65	7.77
CaO	0.68	5.2	1.43	0.6	6.48	1.39	10.8	2.66	9.86	14.2	16.34	8.81
Na_2O	0.43	3.86	2.2	0.35	3.08	7.16	2.3	0.37	2.82	0.92	1.56	3.38
K_2O	15.35	1.89	2.85	4.16	1.8	7.48	0.61	0.09	0.78	0.06	0.07	2.32
TiO_2	0.04	0.516	0.73	0.66	0.67	0.48	0.86	0.2	1.45	0.58	0.055	2.36
P_2O_5	0.12	0.24	0.19	0.16	0.15	0.018	0.15	0.02	0.29	0.007	0.011	0.95
Ba	2418	1020	305	450	317	251	220	46	251	35		527
Ga	11	18.1	21	25.6	16.4	35.8		8	20.7	15.9	13	24.8
Sc	4	9.5	16.6	18.5	19.6	2.22	37.5	29	33.3	24	25	15.2
V	10	94.5	135	87	130	179	216	230	383	175	32	167
Th		2.6	9.9	12.8	4.7	79.3	6		1.3	0.19		6
Pb	5	11.3	18	8.7	19.3	196	25	6	5.5	1.46	6.5	7.2
Ni	7	17	38.5	36.8	142	1.75	85	555	38.8	13.8		140
Co		13.2	14.7	21	30	4.59	40	110	36.3	28	17	47
Rb	530	37.6	116	205	68	130	14	5	13	2.85		37
Sr		790	192	90	252	1160	195		395	435		1100
Y		9.3	30.3	26	18.1	24.7	23	5	27	4.5		22
Zr	33	99	167	96	119	1540	86		98.3	11.6		277
Nb	4	6.8	9.5	14.3	9.8	66.9	10	2	2.3	1.8		68
Cr	12	32.4	58	99	465	3.6	357	20,868	60.4	130	102	134
Cu	19	55.4	40	42	28.6	11.8	84	18	198	11	14	49
Zn	10	71	112	55	62.7	112	81	100	106	48	14	150

the sills is highly differentiated, showing ophitic to sub-ophitic texture. ^{40}Ar–^{39}Ar ages of sills, collected from Pulivendla and Tadpatri, show ages from 1899 ± 20 Ma (Anand *et al.* 2003). Recently, Chakraborty *et al.* (2016) have done a detailed study of lava flows and mafic sills of the Vempalle and Tadpatri Formation of the Papaghni group and Chitravati group, respectively. They reported basaltic lava flows and doleritic sills from the Vempalle Formation and highly differentiated gabbroic sills from the lower part of the Tadpatri Formation. Basaltic lava flows of the Vempalle Formation and sills of Tadpatri Formation are at places vesicular, suggesting their shallow level of emplacement (Chakraborty *et al.* 2016).

A new zone of finely laminated felsic tuff is identified by Sesha Sai (2014) within the intercalated reddish siltstone and dolomite sequence exposed in the lower part of Vempalle Formation in Pulivendela-old Kadiri Road section and a linear zone of pyroclastic rock at the contact between upper part of Vempalle Formation and lower part of the Pulivendla quartzite.

Many dyke swarms occur along the southern, western and northern margins of the Cuddapah basin, showing dominantly three trends, viz., ENE, WNW and N–S. Majority of them are doleritic and some are amphibolite in nature. ^{40}Ar–^{39}Ar and K–Ar ages of dykes range from 1879 to 650 Ma (Anand *et al.* 2003). Sesha Sai (2011) reported picrite and doleritic sills emplaced (along NW–SE direction) between shales and dolerite of Tadpatri Formation.

Igneous activity within Nallamalai group/NFB includes syenite intrusion within the Cumbum Formation at Racherla, Giddaluru and Idamakollu areas and lamproite dykes in Chelima and Zangamrajupalle.

The Racherla syenite is composed of orthoclase, perthite, rebeckite along with apatite, sphene, ilmenite, rutile and biotite as accessory minerals (Rao 2007). The chondrite-normalised rare

Table 4. *Standard used for ICP-MS machine.*

Sl. no.	1	2	3	4	5
Standards	GSD-2	GSD-6	GSD-10	GSD-12	GSD-9
Be	17.1	1.7	0.9	8.2	1.8
Ge	1.7	1.3	0.4	1.87	1.3
Mo	2	7.7	1.2	8.4	0.64
Sn	29	2.8	1.4	54	2.6
La	90	39	13	32	40
Ce	192	68	38	61	78
Pr	18.6	8.4	3.2	6.9	9.2
Nd	62	33	11.8	26	34
Eu	0.49	1.5	0.47	0.61	1.33
Sm	10.8	5.6	2.4	5	6.3
Tb	1.8	0.69	0.42	0.82	0.87
Gd	9.5	5.5	2.2	4.4	5.5
Dy	11	3.8	2.2	4.8	5.1
Ho	2.6	0.76	0.45	0.94	0.96
Er	8.2	2.2	1.3	3.1	2.8
Tm	1.55	0.35	0.2	0.53	0.44
Yb	11	2.1	1.2	3.7	2.8
Lu	1.6	0.34	0.19	0.58	0.45
Hf	20	4.9	1.8	8.3	9.7
Ta	15.3	0.75	0.5	3.2	1.3
W	24	25	1.6	37	1.8
Cs	16.6	9.1	2.3	7.9	5.1
Th	70	9	5	21.4	12.4
Ga	27.4	16.7	6.4	14.1	14
Y	67	20	14	29	27
Zr	460	170	70	234	370
Nb	95	12	6.8	15.4	18

earth element (REE) pattern of Racherla syenite is characterised by high light rare earth element/heavy rare earth element (LREE/HREE) ratio. The age of Racherla syenite is 1326 ± 73 Ma (Rao 2007). High incompatible trace elements (Zr/Nb, La/Nb) and high LREE/HREE ratios of Racherla syenite suggest its origin from an enriched mantle source (Rao *et al.* 2012).

Chelima lamproite dykes are located 1 km south of Chelima town and cover an area of 3 km^2. The thickness of the dykes ranges from 1 to 5 m and have been mined for diamond since ancient time (Rao 2007). The Chelima dykes are silica under-saturated, with K_2O content ranging from 1.05 to 3.61% as well as K_2O/Na_2O ratio >3. Chelima dykes are strongly enriched in LREE with La abundances being 1000 times of chondrite and HREE abundances 20 times of chondrite. Strongly LREE-enriched chondrite-normalised REE plot of Chelima lamproite suggests that the source for these lamproites is a metasomatised mantle (Rao 2007), although the mechanism of metasomatism is not explained. K–Ar (phlogopite) age of Chelima dykes vary from 1328 ± 52 to 1380 ± 54 Ma (Rao 2007). Lamproitic dykes of Zangamrajupalle are similar to Chelima dykes in petrology and geochemistry but are of much younger age (1090 Ma; Anil *et al.* 2001).

This study area is located at the southernmost part of NFB, in Pullampet sub-basin, in the vicinity of Rajampet town (figure 1).

3. Field relation and petrography

The newly found intrusive dolerite dykes and sills are located within the shale of Cumbum Formation of NFB near Gattuvaripalle village (N14°15′33.04″ and E79°15′42.69″, figure 2a). The dykes are undeformed and cut across/subparallel to the S_1 schistosity of shale (figure 2b), but the sills are deformed and have a strong development of schistosity, which is parallel to the regional S_1 schistosity of shale (figure 2c). A total of five numbers of dykes are encountered showing bouldery outcrop pattern. Two dykes trend ENE–WSW, and their length is >1 km, but the other three dykes are NNW–SSE trending and are of variable length. The dimension of sills is very less, and only three sills (maximum length 15 m and thickness 5 m) can be demarcated on map (figure 2a). The upper parts of the dykes are at places vesicular, filled by quartz, calcite and chlorite, suggesting very shallow depth of emplacement.

A microscopic study reveals that both dyke and sills are doleritic in composition, and the main constituents are clino-pyroxene, plagioclase, with very low amount of magnetite, spinel and little quartz. Dyke and sills contain an average modal amount of 58% pyroxene and 42% plagioclase. Both pyroxene and plagioclase grains have suffered hydrothermal alteration. Pyroxene grains are altered to fibrous chlorites (figure 2d), whereas plagioclase is altered to either epidote or sericite. Dykes show ophitic (figure 2e), subophitic and inter-granular (figure 2f) texture. Unaltered pyroxene grains in dyke show irregular grain boundary and intra-granular fracture. Two sets of cleavage are preserved in basal section of clinopyroxene grains (figure 2g). Plagioclase feldspar is lath shaped. Unaltered pyroxenes are rarely visible in sill samples, and most of the grains have converted to fibrous chlorite (figure 2h). Evidence of deformation like C′ type of shear bands (showing dextral sense of shearing; figure 2i) and undulate

Table 5. *Major oxide (all values in wt.%), trace elements (all values in ppm) and REE values of mafic dyke and sills.*

Sample	11/RJM/14	17/RJM/14	17A/RJM/14	18/RJM/14	100/RJM/14	115/RJM/14
Latitude, longitude	N14°16′35.7″, E79°18′05.2″	N14°15′35.4″, E79°17′53.9″	N14°15′34.3″, E79°17′53.5″	N14°15′44.3″, E79°17′51.7″	N14°16′35.6″, E79°18′20.4″	N14°16′58.1″, E79°19′22.2″
	Dyke	Dyke	Dyke	Dyke	Dyke	Dyke
Ba	318	383	370	401	559	318
Co	48	52	46	46	55	52
Cr	180	180	169	169	191	171
Cu	39	48	47	46	37	55
Ga	13	6.4	11	10	14	14
Nb	5.8	6.5	5.6	5.9	5	5
Ni	68	64	57	74	110	64
Pb	25	11	26	96	38	10
Rb	48	37	42	50	39	41
Sc	33	29	34	31	30	28
Sr	243	294	246	327	206	148
Th	4	5	<4	10	<4.0	<4.0
V	250	265	275	251	235	256
Y	13	14	13	13	13	13
Zn	105	82	93	85	147	100
Zr	85	81	82	101	63	75
La	14.98	12.32	13.51	21.01	11.282	14.102
Ce	37.03	29.39	33.07	52	25.065	80.506
Pr	4.35	3.7	3.95	5.91	3.413	4.159
Nd	17.67	15.26	16.08	23.46	15.068	18.413
Eu	1.27	1.12	1.28	1.65	1.301	1.245
Sm	4.09	3.63	3.87	5.25	3.519	4.116
Tb	0.65	0.64	0.65	0.81	0.598	0.701
Gd	3.96	3.79	3.92	5.07	3.918	4.415
Dy	3.97	3.72	3.91	4.93	3.486	4.097
Ho	0.74	0.7	0.74	0.92	0.667	0.77
Er	2.1	1.94	2.06	2.58	1.864	2.069
Tm	0.31	0.28	0.29	0.39	0.285	0.327
Yb	1.93	1.74	1.84	2.43	1.627	1.867
Lu	0.31	0.28	0.27	0.38	0.269	0.301
Be	3.66	3.22	3.58	5.38	2.93	4.263
Ge	0.15	0.31	0.28	0.48	0.563	0.287
Mo	14.98	12.32	13.51	21.01	11.282	14.102
Cs	37.03	29.39	33.07	52	25.065	80.504
Hf	4.35	3.7	3.95	5.91	3.413	4.159
Ta	0.15	0.31	0.28	0.48	0.56	0.28
W	<5	<5	<5	<5	<5	<5
Bi	<0.1	<0.1	<0.1	<0.1	<0.1	<0.1
U	1.44	1.1	1.19	1.84	0.691	0.635
$(La/Sm)_n$	2.36	2.19	2.25	2.58	2.07	2.21
$(Gd/Yb)_n$	1.7	1.8	1.76	1.73	1.99	1.96
Ce/Ce*	1.12	1.07	1.11	1.14	0.99	2.58
La/Nb	2.58	1.895	2.4125	3.561	2.2564	2.8204
SiO_2	48.65	48.37	48.62	45.34	46.95	47.52
MgO	7.83	8.25	7.59	7.09	9.28	7.22
Fe_2O_3	14.74	14.69	14.8291	15.34	15.67	15.44
Al_2O_3	13.4	12.55	12.85	15.38	12.65	14.77
CaO	7.33	7.58	7.44	7.15	7.19	5.63
MnO	0.15	0.16	0.18	0.17	0.2	0.15
Na_2O	1.43	1.31	1.3	1.02	1.47	1.48

Table 5. *(Continued.)*

Sample	11/RJM/14	17/RJM/14	17A/RJM/14	18/RJM/14	100/RJM/14	115/RJM/14
Latitude, longitude	N14°16′35.7″, E79°18′05.2″	N14°15′35.4″, E79°17′53.9″	N14°15′34.3″, E79°17′53.5″	N14°15′44.3″, E79°17′51.7″	N14°16′35.6″, E79°18′20.4″	N14°16′58.1″, E79°19′22.2″
K_2O	1.53	1.24	1.32	1.75	1.38	1.23
TiO_2	1.23	1.14	1.39	1.6	1.12	1.19
P_2O_5	0.13	0.12	0.12	0.1	0.14	0.1
LOI	2.885	4.008	3.537	4.256	3.23	4.56
Mg#	0.55	0.57	0.54	0.52	0.58	0.52
	Sill	Sill	Sill	Sill	Dyke	
Ba	238	558	180	450	433	
Co	45	47	52	38	53	
Cr	141	183	194	157	197	
Cu	72	49	38	42	60	
Ga	11	8.6	14	9.6	14	
Nb	6.4	5	5.3	5	5.2	
Ni	37	66	70	44	64	
Pb	11	24	12	8.3	22	
Rb	47	37	33	58	33	
Sc	35	33	29	33	32	
Sr	216	241	185	98	183	
Th	<4.0	<4.0	<4.0	<4.0	<4.0	
V	289	258	253	271	264	
Y	12	13	12	12	13	
Zn	104	99	99	75	113	
Zr	95	66	60	84	71	
La	17.163	12.408	13.664	22.009	22.549	
Ce	39.37	25.869	29.312	36.911	46.023	
Pr	4.975	3.513	3.976	5.013	5.823	
Nd	20.948	15.291	17.454	21.347	23.837	
Eu	1.3954	1.252	1.336	1.448	1.55	
Sm	4.4881	3.618	3.815	4.941	5.166	
Tb	0.77	0.621	0.677	0.772	0.804	
Gd	5.096	3.853	4.171	5.111	5.3	
Dy	4.474	3.595	3.81	4.461	4.67	
Ho	0.872	0.695	0.736	0.835	0.884	
Er	2.231	1.858	1.961	2.221	2.354	
Tm	0.37	0.29	0.315	0.32	0.359	
Yb	2.152	1.733	1.789	2.064	2.339	
Lu	0.346	0.275	0.301	0.328	0.372	
Be	4.413	3.197	3.317	3.262	3.707	
Ge	0.497	0.33	0.539	0.459	0.5745	
Mo	17.163	12.408	13.664	22.009	22.549	
Cs	39.37	25.869	29.311	36.91	46.023	
Hf	4.975	3.513	3.976	5.013	5.823	
Ta	0.33	0.53	0.45	0.49	0.57	
W	<5	<5	<5	<5	<5	
Bi	<0.1	<0.1	<0.1	<0.01	<0.01	
U	0.758	0.569	0.695	0.705	1.017	
(La/Sm)n	2.47	2.21	2.31	2.88	2.82	
(Gd/Yb)n	1.96	1.78	1.93	2.05	1.87	
Ce/Ce*	1.04	0.96	0.98	0.86	0.98	
La/Nb	2.681	2.481	2.578	4.401	4.336	
SiO_2	52.05	48.15	47.45	49.87	44.28	
MgO	6.57	8	8.4	7.86	8.68	

Table 5. *(Continued.)*

Sample	FG/142/RJM/14	146/RJM/14	149/RJM/14	341A/RJM/15	375/RJM/14
Latitude, longitude	N14°16′38.6″, E79°18′33.4″	N14°16′41.2″, E79°18′49.2″	N14°16′35.0″, E79°19′12.0″	N14°16′31.7″, E79°18′21.2″	N14°16′34.0″, E79°19′12.4″
Fe_2O_3	15.8	14.85	15.03	16.75	18.26
Al_2O_3	12.31	12.85	12.7	11.38	10.48
CaO	4.56	8.09	7.5	3.02	8.42
MnO	0.13	0.16	0.18	0.14	0.15
Na_2O	1.25	1.54	1.6	1.63	1.45
K_2O	1.49	1.26	0.89	1.82	1.96
TiO_2	0.88	1.09	1.2	0.81	1.28
P_2O_5	0.15	0.14	0.1	0.15	0.13
LOI	4.05	3.16	4.4	6.57	5.26
Mg#	0.51	0.55	0.57	0.53	0.53

extinction of quartz grains are observed in mafic sills, whereas in dyke samples, deformational evidences are lacking. It suggests that the sills are older than dykes and have intruded prior to D_1 phase of deformation. Electron probe micro-analyser (EPMA) study was carried out by Cameca SX-100 machine in GSI, EPMA lab, Hyderabad, using 15 keV accelerating voltage and 20 nA current (was carried out for dyke samples only as sill samples are highly altered). TAP, PET, LLIF and LIF are the spectrometers used for the silicate analysis. EPMA data reveal that all pyroxene grains are augite in composition (table 2), and feldspars are albitic (albitised) in composition (table 2). Close inspection of clino-pyroxene composition (table 2) reveals that there are two types of clino-pyroxene, one is low in CaO and MgO but high in FeO (CaO and MgO value ranging from 12 to 14%) and another is high in CaO and MgO but low in FeO (CaO and MgO value ranging from 17 to 19%). Pyroxene thermometry after Lindsley (1983) shows that except three all the Cpx grains form two distinct clusters (one Ca rich and one Ca poor) and plot between contours of 1100°C and 1200°C (figure 2j).

4. Geochemistry

4.1 *Major and trace element geochemistry*

A total of 11 (7 dyke and 4 sill samples) samples of dyke and sill were analysed for major oxide, trace element and REE in Chemical Division, GSI, Hyderabad. Major and trace elements were analysed by X-ray fluorescence (XRF) method in PAN Analytical MagiX machine, and SuperQ Manager software was used for analysis. The standards used for major oxide and trace element analysis are represented in table 3. Agilent 7700× inductively coupled plasma mass spectrometry (ICP-MS) was used for determining REE concentration in rock, and the standards used for REE analysis are given in table 4.

SiO_2 and MgO content of dykes and sills varies from 45 to 52 and 6.5 to 9.28 wt.%, respectively (table 5). Mg# values of dykes and sills range from 0.51 to 0.58 (table 5) and Ni values from 37 to 110 ppm (table 6) indicating their non-primitive (highly fractionated) nature. Al_2O_3 values range from 12.31 to 15.38 wt.% suggesting low alumina-type basalt. The rocks are sub-alkaline (molar $Na_2O + K_2O/Al_2O_3 < 1$) in nature.

In $Nb/Y–Zr/TiO_2$ bivariate plot (after Winchester and Floyd 1977), all the samples occupy sub-alkaline basalt field (figure 3a). In AFM plot (Irvine and Baragar 1971), all the samples fall in tholeiitic field showing an iron enrichment trend (figure 3b). FeO*/MgO *vs.* SiO_2 bivariate diagram also (figure 3c, after Miyashiro 1974) confirms their tholeiitic nature. In triangular plot (figure 3d) after Jensen (1976), all samples straddle the boundary between high Fe tholeiite basalt field and high Mg tholeiite basalt field, and only one sample fall in komatiitic basalt field.

Bivariate plot (only of dyke samples as sill samples are very low in number and do not show any recognisable trend) of MgO *vs.* Al_2O_3 and TiO_2 (figure 4a and b) shows a linear negative

Table 6. *Discriminant function using TecD software by Verma and Verma (2013).*

Sample ID	(IA-MORB-CRB+OIB)t		(IA-OIB-CRB)t		(IA-MORB-OIB)t		(IA-MORB-CRB)t	
	DF1	DF2	DF1	DF2	DF1	DF2	DF1	DF2
11/RJM/14	− 3.235830648	− 2.147662425	− 4.064461328	− 0.697022743	− 2.649796901	− 1.751775828	− 2.904869241	− 2.018095824
17/RJM/14	− 2.99703728	− 1.975315749	− 3.955449822	− 0.595245449	− 2.420137757	− 1.677440777	− 2.688674594	− 1.837097785
17A/RJM/14	− 3.31507133	− 2.17124358	− 4.200772375	− 0.60556545	− 2.730442512	− 1.772477714	− 2.977246441	− 2.04332259
18/RJM/14	− 3.240543698	− 2.151583834	− 3.810391482	− 0.805223441	− 2.635768818	− 1.70118364	− 2.883448652	− 2.048151053
100/RJM/14	− 3.508764869	− 2.342212468	− 4.540981432	− 0.346922212	− 2.940925397	− 1.914315681	− 3.125609672	− 2.243079298
145/RJM/14	− 2.974905035	− 2.410845956	− 5.506549545	− 0.109262334	− 2.560369509	− 2.341088369	− 2.76573149	− 2.16301782
146/RJM/14	− 3.543204477	− 2.302415666	− 4.488360428	− 0.576403702	− 2.96000623	− 1.855916708	− 3.199168573	− 2.167264611
149/RJM/14	− 3.397066319	− 2.271722574	− 4.307452751	− 0.633325077	− 2.818668865	− 1.844137818	− 3.054163171	− 2.143203891
375/RJM/15	− 3.210125072	− 2.237093181	− 3.805897591	− 0.970243525	− 2.617170007	− 1.773868933	− 2.870181788	− 2.118327283

trend suggesting late crystallisation of plagioclase and ilmenite. Plot of CaO *vs.* MgO (figure 4c) shows a linear positive trend suggesting early crystallisation of clino-pyroxene. Fe_2O_3 *vs.* MgO do not show any recognisable trend (figure 4d). In Ni, Co and Cr *vs.* MgO bivariate plots, Cr shows good positive correlation with MgO compared to Ni and Co suggesting lack of olivine and mostly pyroxene and spinel fractionation (figure 5a–c). Bivariate plots of Zr *vs.* high-field strength (HFS) elements (Nb and Hf) show a linear positive trend, indicating their co-genetic nature (figure 5d and e).

4.2 *REE geochemistry*

Chondrite-normalised REE plots (after Sun and McDonough 1989) of dyke and sills show that the rocks are enriched in LREE with comparison to HREE (figure 6a). The relatively shallow slope of HREE (figure 6a) suggests the absence of garnet in source rock. The absence of Eu anomaly may be due to albitisation of plagioclase. $(Gd/Yb)_N$ ratio varies from 1.70 to 2.05 (table 5), suggesting melting above garnet stability field. Plots (samples of basic dykes and sills) in MORB-normalised multi-element diagram (normalising values after Pearce 1983) show that large-ion lithophile (LIL) elements are strongly enriched with respect to HFS element with prominent trough in Nb, Ta, Zr and Y and peaks in Rb, Ba, Ce, Hf and Th suggesting their enriched nature (figure 6b). A primitive mantle-normalised multi-element diagram (normalising values after Sun and McDonough 1989) shows prominent peaks in Pb, U, Cs and K; slight peaks in Nd and Sm; and prominent troughs in Nb, Y, Ti and Zr (figure 6c). Enrichment in LREE and LIL elements can occur either by low degree of partial melting or by crustal contamination. Zr/Sm ratio of 15–21, La/Sm ratio of 3.3–4.4, La/Yb ratio of 7–10.6 and Ce/Yb ratio 15.4–21.6 for present samples with comparison to Achaean Upper Continental Crust (31, 4, 10 and 21, respectively, Khanna 2013) suggest limited crustal contamination. $(La/Sm)_N$ ratio (normalisation values after Sun and McDonough 1989) of the samples (2.07–2.88, table 5) are quite low in comparison to average continental crust (∼4.25, Srivastava and Singh 2004) and Cuddapah basin granites (25–30, Anand *et al.* 2003) suggesting lack of crustal contamination. Despite their relative age difference, the dyke and sills are very

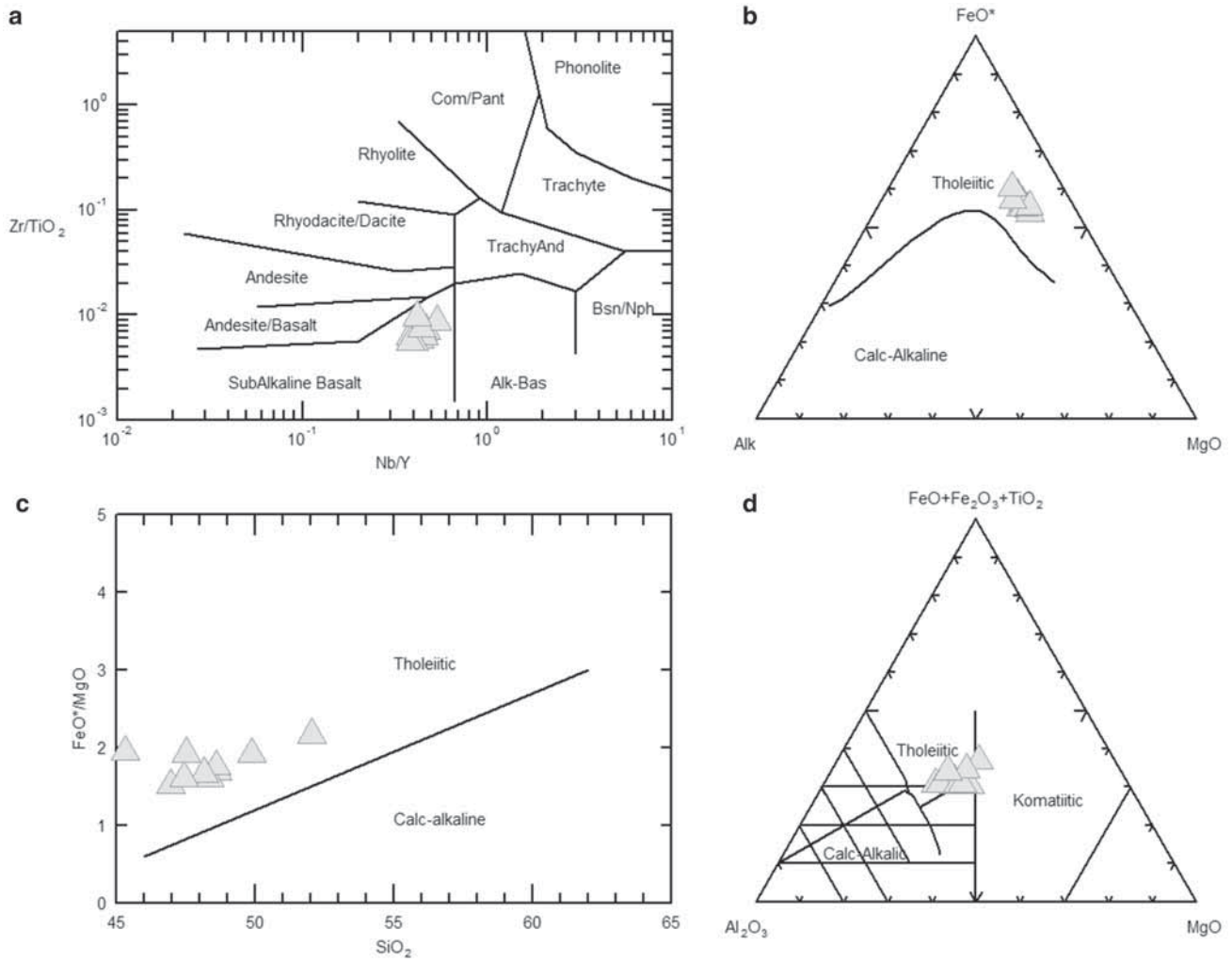

Figure 3. (**a**) Plots of dyke and sill samples in Nb/Y–Zr/TiO_2 bivariate plot after Winchester and Floyd, (**b**) plots of dyke and sill samples in AFM diagram after Irvine and Baragar (1971), (**c**) bivariate plot after Miashiro (1974) showing tholeiitic nature of rocks and (**d**) triangular plot after Jensen (1976).

much similar in their geochemical character, suggesting generation from a similar source at different phases.

5. Tectonic setting of dyke and sills

Mobility of elements due to metamorphism and hydrothermal alteration is a problem in amphibolite facies metamorphic condition (Rajamani *et al.* 1989; Vijay Kumar *et al.* 2006). Rb, Sr and Ba are considered to be more mobile than Ti, Zr, Nb, Y and REE (Srivastava 2012). Zr is thought to be the most immobile element (Srivastava 2012). Present dyke and sills are not metamorphosed, but evidences of hydrothermal alteration are observed during petrographic study. In CaO/Al_2O_3–MgO–SiO_2 triangular plot (Schweitzer and Kröner 1985),

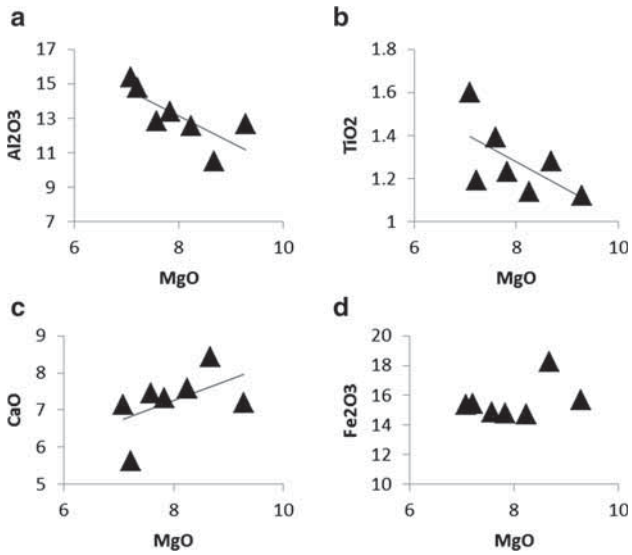

Figure 4. (**a**–**d**) Plots in Harker diagram for dyke samples.

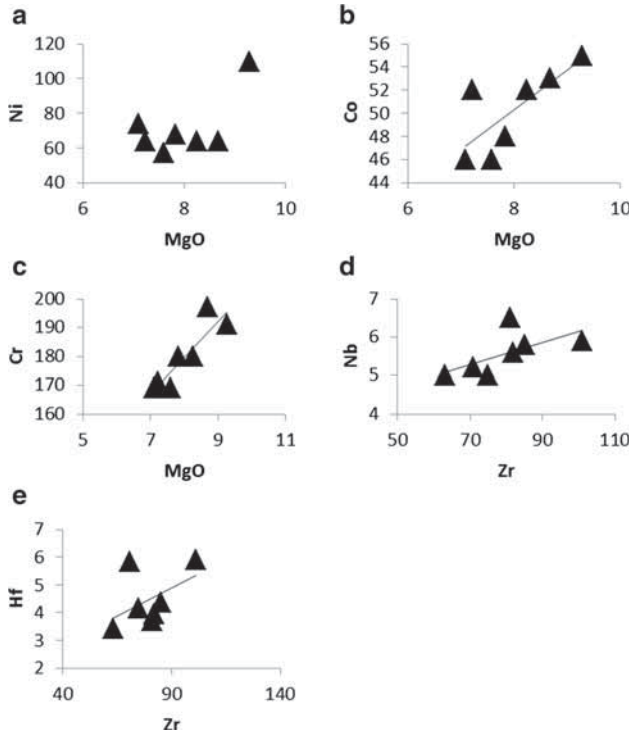

Figure 5. (**a**–**c**) Bivariate plot of Ni, Cr and Co with respect to MgO for dyke and sill samples and (**d** and **e**) bivariate plots of Zr *vs.* Hf and Nb.

except two, all samples fall in unaltered field (figure 6d). Samples with Ce/Ce* values between 0.95 and 1.1 are considered to be showing minimal REE mobility and samples with Ce/Ce* values outside this range indicate high REE mobility (Manikyamba *et al.* 2015). In the present case, only two samples (table 5) fall outside this range (table 5) suggesting negligible LREE mobility.

Keeping in view the altered nature of samples, we have used immobile element-based (like Ti, Nb, Zr, Cr, Y and LREE) plots for tectonic discrimination. Tectonic discrimination diagram using Ti, Zr and Y (after Pearce and Cann 1973) shows that all the samples fall in a within-plate basalt field (figure 7a), while in Cr *vs.* Y bivariate diagram (after Pearce 1982), all the samples occupy the volcanic arc basalt field (figure 7b). In plots of dyke–sill samples in probability-based immobile trace element tectonic discrimination diagrams (using TecD software after Verma and Gómez 2013) for basic rocks (after Agrawal *et al.* 2008) which use discriminant functions (of log-transformed immobile trace elements) to reduce the number of variables into two dimensions, all the samples fall in island arc field (figure 7c). The values of discriminant functions are given in table 6. Tectonic discrimination diagram based on immobile trace elements Nb, Zr and Y (after Meschede 1986) shows (figure 7d) that most of the samples fall in C field and some fall in A-II field suggesting volcanic arc character and within-plate tholeiite, respectively.

6. Trace element modelling

Forward geochemical modelling has been carried out for estimating the approximate degrees of melting required from a source (spinel peridotite) to generate the observed compositions of dyke and sills. Only REE values of the samples were chosen for modelling because of their relatively immobile nature. The modelling was done using a Microsoft Excel spreadsheet, PETROMODELLER (ERSOY 2013). The REE concentration for the assumed source was selected from Sharkov *et al.* (2016, sample no. -819-17). The normalised REE pattern of the assumed source is also enriched in LREE relative to HREE (figure 8a). Mineral mode D_i (spinel peridotite containing olivine 57%, Opx 25.5%, Cpx 15.0% and spinel 2.5%) and melting mode (P_i) values are after Kostopoulos (1991), and distribution coefficient (K_d) values are after Shaw (2007). Our modelling shows that (figure 8a) nearly 8% batch melting (melting equations after ERSOY 2013) from an enriched spinel peridotite produces a normalised REE pattern which approximately matches the actual normalised REE pattern of the samples. If we assume primitive mantle peridotite as a source composition (after Palme and O'Neill 2014), the resulting normalised REE pattern after 8% of batch melting is flat with no inter-REE fractionation and do not corroborate with the actual normalised REE pattern of the samples (figure 8b).

The hypothesis that the dyke and sills are generated from an enriched source has also been tested by applying the inversion modelling technique (after Feigenson *et al.* 1996) to the REE data of dyke and sills. Inversion modelling gives an idea of the REE pattern of the original source rock (spinel peridotite in this case) from which the magma was generated by partial melting. The result of inversion modelling (after Feigenson *et al.* 1996) using REE data of dyke and sills (by using IGPET software) shows that the source had an enriched LREE and flat HREE pattern indicating garnet-free enriched spinel peridotite source (figure 8c).

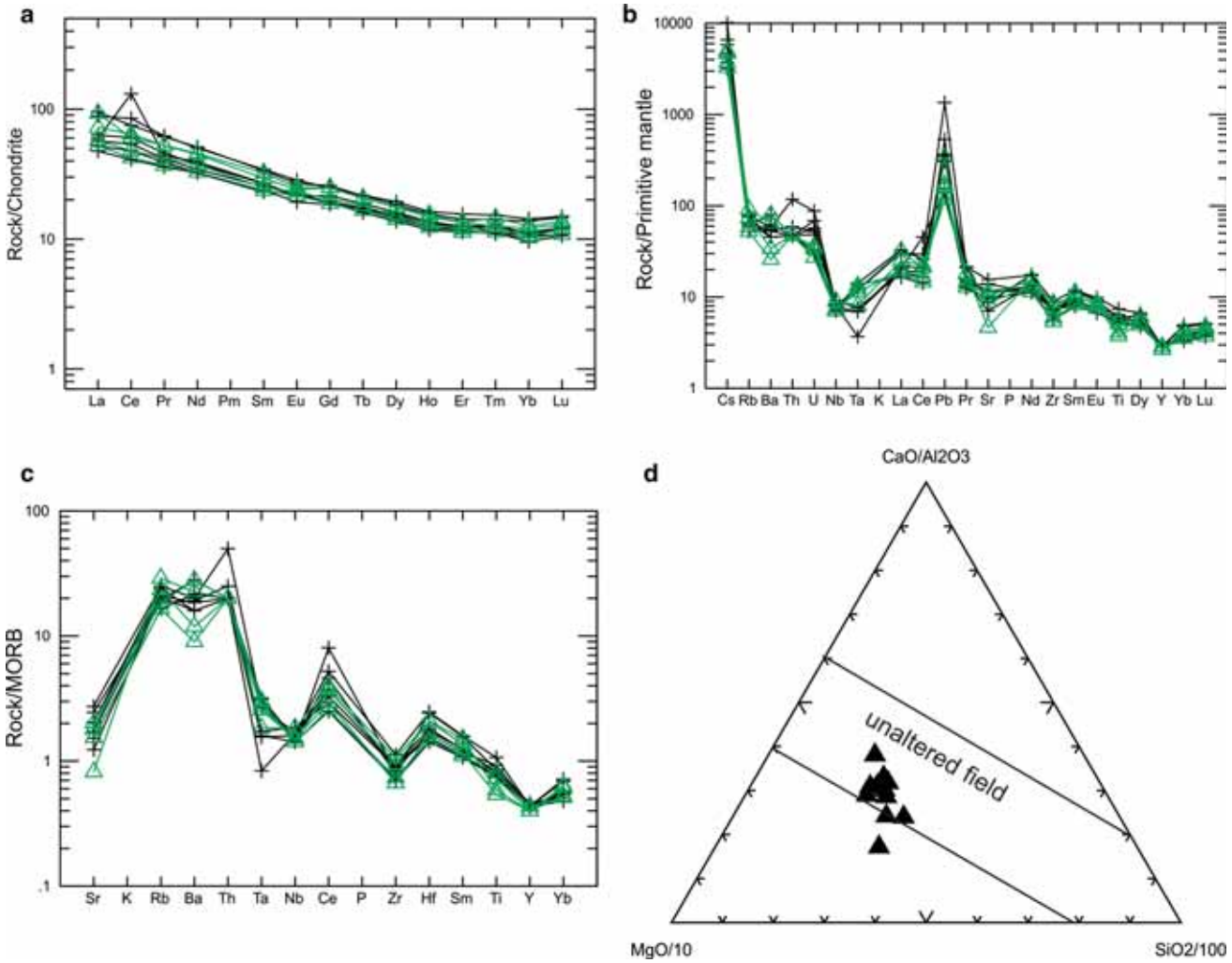

Figure 6. (**a**) Chondrite-normalised plot of REE of both dyke and sill (normalising values after Sun and McDonough 1989). (**b**) Primitive mantle-normalised plot of dyke and sill samples (normalising values after Sun and McDonough 1989). Green line representing sills and black line dykes. (**c**) MORB normalised plot of both dyke and sill samples (after Pearce and Cann 1973). (**d**) $CaO/Al_2O_3-MgO-SiO_2$ triangular diagram after Schweitzer and Kröner (1985).

7. Discussion and conclusion

Chakraborty *et al.* (2016) have suggested a strongly metasomatised mantle for the origin of Tadpatri sills and indicated towards a possible role of mantle plume in mantle rifting and metasomatism. The lamproite dykes of Chelima, Zangamrajupalle and Racherla syenite are also generated from a highly metasomatised mantle (Rao 2007). Rao *et al.* (2004) have advocated against the contribution of mantle plume in the generation of Proterozoic kimberlites and lamproites in and around Cuddapah basin and suggested extension of variably thick lithosphere during mid-Proterozoic. Rao *et al.* (2004) have further suggested that an episode of depletion prior to enrichment of the subcontinental lithospheric mantle was necessary for the generation of kimberlites and lamproites in and around Cuddapah basin.

Saha and Tripathy (2012) have discussed in detail about the sedimentary nature of both undeformed Cuddapah (Papaghni and Chitravati groups) and NFB. Papaghni and Chitravati groups represent an intra-cratonic basin, while the sediments of Nallamalai group show evidences of tidal and storm activity and were deposited in a marginal basin connected to a Palaeoproterozoic ocean (Saha and Tripathy 2012). As stated earlier, Nallamalai group is separated from undeformed Cuddapah basin by an easterly dipping intra-continental thrust (Maidukuru thrust) and from NSB by Velikonda thrust. Deep seismic sounding profiles also indicate two major faults at the western and eastern boundaries of NFB

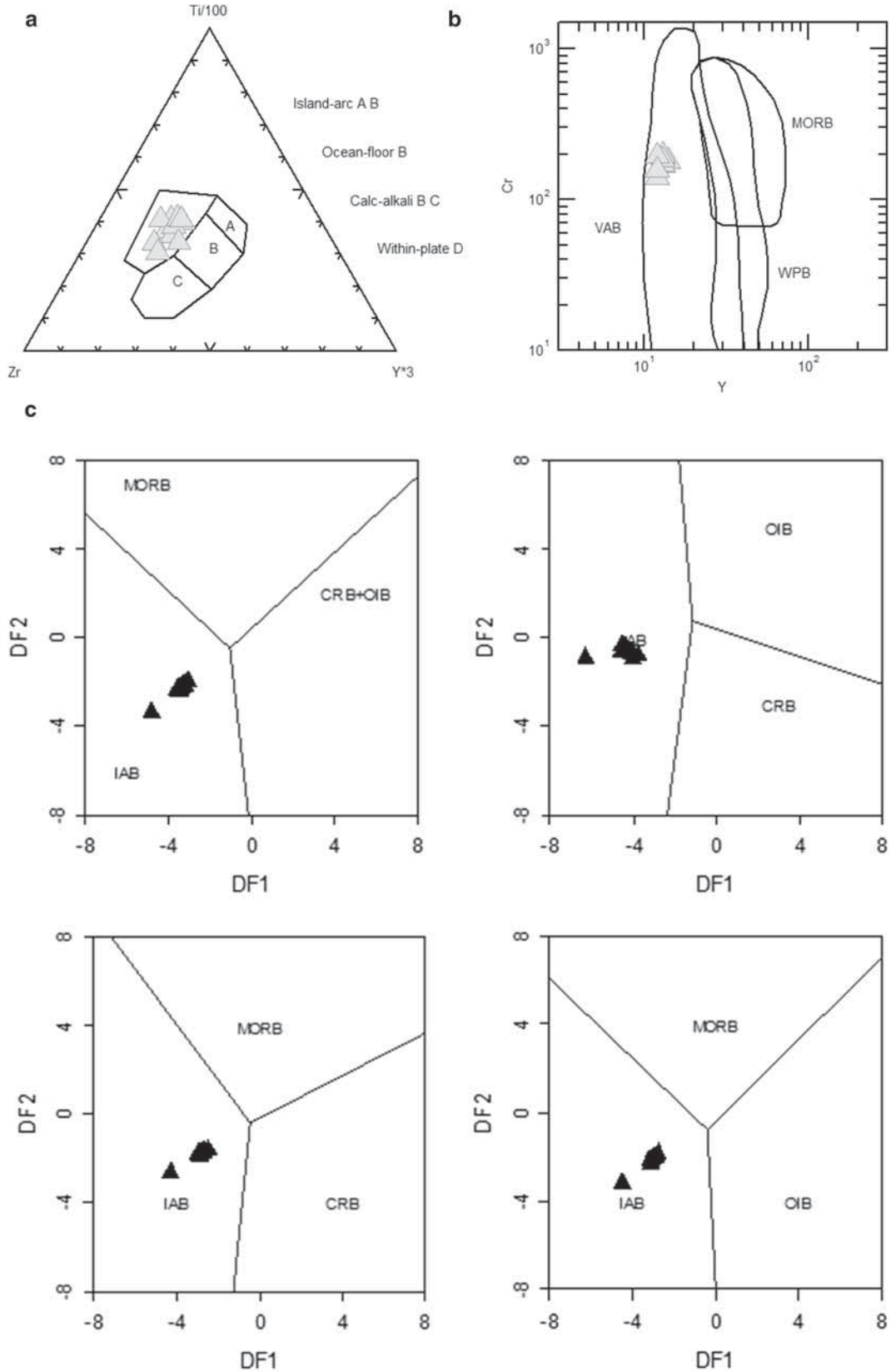

Figure 7. (**a**) Tectonic discrimination diagram after Pearce and Cann (1973), (**b**) bivariate tectonic discrimination diagram after Pearce (1982), (**c**) probability-based trace element tectonic discrimination diagrams (used for basic and ultrabasic rocks only) after Agrawal *et al.* (2008) and (**d**) triangular tectonic discrimination diagram based on immobile trace elements Nb, Zr and Y after Meschede (1986).

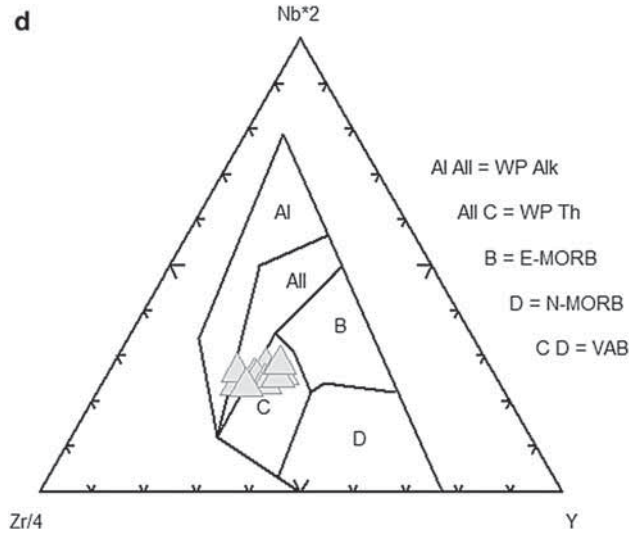

Figure 7. (*Continued.*)

which offsets the moho (Saha and Tripathy 2012). Based on these evidences, Saha and Tripathy (2012) suggested an allocthonous nature of the NFB, which was deposited far east, separately from undeformed Cuddapah basin. As discussed earlier, the adjoining NSB shows evidence of intra-oceanic plate convergence at 1.9 and 1.3 Ga in terms of KOM and KOC. Vinjamuru group rocks of NSB were generated in an island arc setting during 1.6 Ga due to westward plate convergence. NFB formed at the outer margin of this island arc archipelago far away from the eastern margin of the EDC. Hence, the mantle beneath NFB is supposed to get enriched by subduction-derived fluids during multiple convergences and subduction phenomenon. Whereas Cuddapah and Kurnool basins were originated at the eastern margin of EDC in a passive margin setting.

Plot of our mafic dyke and sill samples in tectonic discrimination diagrams shows contrasting results, as some plots indicate within-plate tectonic environment, while others suggest a subduction zone/arc character for the rocks. Plots in a primitive mantle-normalised multi-element spider diagram (figure 6b) show troughs in Nb, Ta, Ti and Zr which are characteristic of subduction zone environment, although these signatures can also generate by crustal contamination. Available evidences suggest very limited influence of crustal contamination. Field evidences and their very small aerial extent indicate that the dyke and sills must have been generated by lithospheric extension and not by subduction zone activity. La/Nb ratio >1 is considered as a signature for subduction-related basalts (Goodenough *et al.* 2002). The La/Nb ratio for the present samples varies from 1.89 to 4.4 (table 5). Results of both forward and inversion geochemical modelling of the dyke and sill samples indicate their generation from an enriched spinel peridotite mantle. The absence of crustal contamination signatures point towards a possibility that these mafic dyke and sills might have been generated from a mantle which got enriched by an earlier subduction-related activity (during formation of Vinjamuru group around 1.6 Ga) and was subjected to extension at a later phase. Similar geochemical signatures of basaltic dykes from Garder province of South Greenland were explained by Goodenough *et al.* (2002) due to their generation from previously subduction-enriched mantle. The paradox of subduction signatures in a within-plate setting can be explained by the fact that the magma of dyke and sills inherited the chemical characteristics of the subduction-enriched source region. But in the absence of isotope data, it is not possible to conclude with absolute certainty. The above hypothesis is also in conformity with the view that NFB was generated away from the EDC in an active margin setting. We have also noted the occurrence of acid tuffs and volcanics in the immediate vicinity of the dyke and sills, occurring within the shale of Cumbum Formation, which show collision margin tectonic character (Das and Chakraborty, GSI, unpublished report, 2015; Chakraborty and Das 2016) suggesting that NFB was generated in an active margin setting. Sheppard *et al.* (2017) dated monazite grains at 531 ± 7 Ma from a low-grade metasedimentary rock from Mangampeta barite mine situated in the southern part of NFB. The monazite grains grew during D_1 phase of deformation, thus constraining the age of D_1 deformation of NFB to be Pan-African. As the sills suffered D_1 deformation, they are supposed to be older than Pan-African event, whereas the undeformed dykes are younger than Pan-African event. The absence of age data of the dyke and sills is a major constraint in linking them to any global tectonic event.

So, from the above discussion, it can be said that the mafic dyke and sills, which intruded at different phases into the Cumbum Formation of Nallamalai group, are highly fractionated sub-alkaline tholeiite, generated in a within-plate setting by lithospheric extension possibly from a previous subduction-enriched (metasomatised) spinel peridotite by nearly 8% of partial melting.

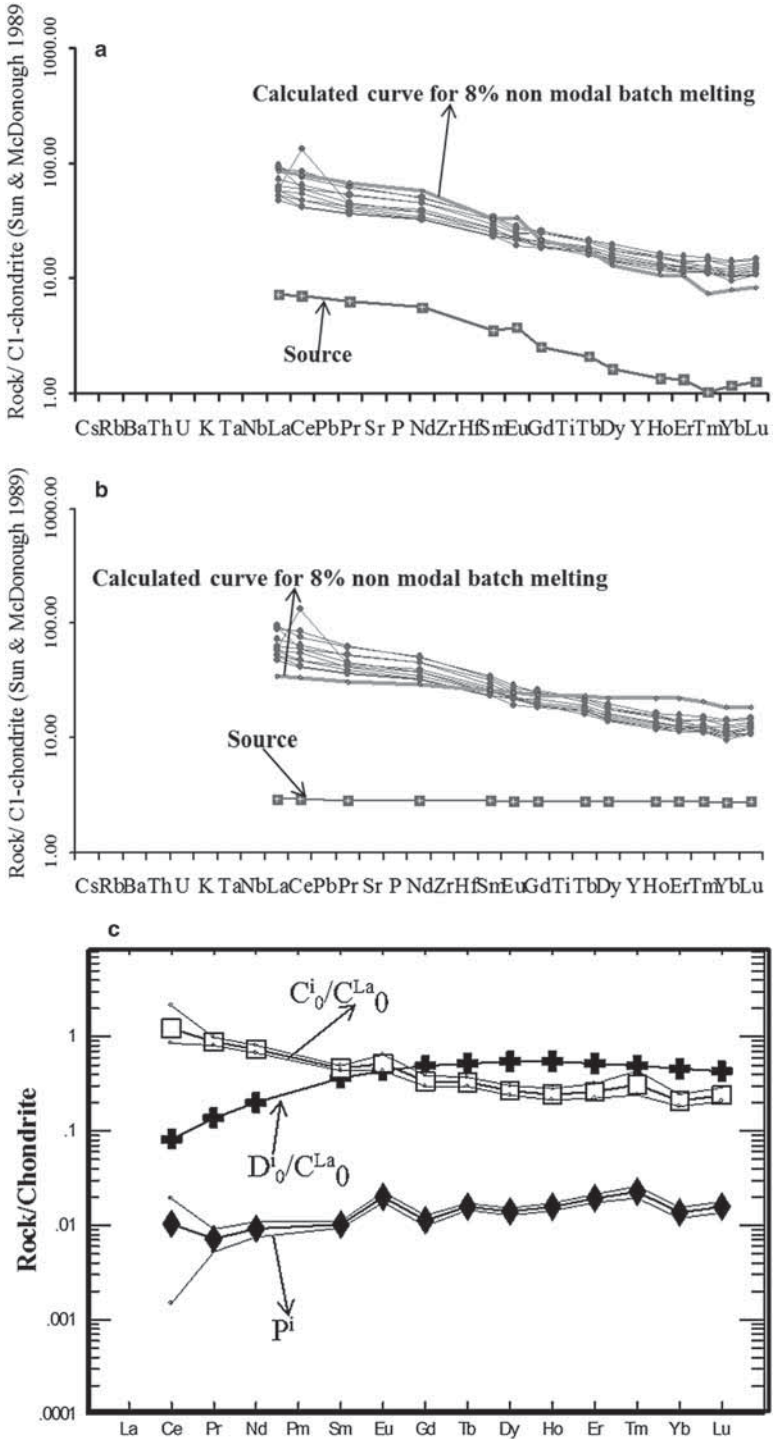

Figure 8. (**a**) Forward geochemical modelling showing that the observed normalised REE concentration of the mafic dyke and sills can be achieved by 8% non-modal batch melting of an enriched source (composition of source REE is taken from Sharkov *et al.* 2016), containing olivine: 57%, Opx 25.5%, Cpx 15.0% and spinel 2.5%, and melting mode (P_i) after Kostopoulos (1991; olivine 5%, Opx 15%, Cpx 60% and Sp 20%). (**b**) Forward geochemical modelling showing that the observed normalised REE concentration of the mafic dyke and sills cannot be achieved by 8% non-modal batch melting of an primitive mantle source (composition of source REE are taken from Palme and O'Neill 2014), containing olivine: 57%, Opx 25.5%, Cpx 15.0% and spinel 2.5%, and melting mode (P_i) after Kostopoulos (1991; olivine 5%, Opx 15%, Cpx 60% and Sp 20%). (**c**) Inverse geochemical modelling (after Feigenson *et al.* 1996) showing that the source of the observed dyke and sill was also enriched in LREE relative to HREE. Mineral mode (D_i) and melting mode (P_i) after Kostopoulos (1991; olivine 5%, Opx 15%, Cpx 60% and Sp 20%). The range of P_i values has been given as input. C_i indicates initial concentration of an element in the source and D_{i0} indicate initial bulk partition coefficient of an element in the source. Relatively constant D_0 (bulk partition coefficient) in middle rare earth element (MREE) and HREE values indicate a garnet-free source.

Acknowledgements

It is indeed a pleasing privilege for the authors to express their profound gratefulness to Shri S Kannan, then-Deputy Director General and HOD, GSI, SR, Hyderabad, and the authors are most grateful and indebted to Shri P A Ramesh Babu, then-Deputy Director General, SU: AP, GSI, SR, Hyderabad, for his sustained interest, warm encouragement and valuable suggestions. The authors pay their obeisance to Shri S M K Kazimi (then-project director) for his insurmountable enthusiasm, expert supervision and excellent guidance. The authors are indebted to EPMA Laboratory, GSI, SR, Hyderabad, for providing high-quality EPMA data. The authors acknowledge Dr V B Damodar Rao, Sr Chemist of Chemical Division, GSI, SR, for carrying out the chemical analysis of the samples.

References

Agrawal S, Guevara M and Verma S P 2008 Tectonic discrimination of basic and ultrabasic rocks through log-transformed ratios of immobile trace elements; *Int. Geol. Rev.* **50** 1057–1079.

Anand M, Gibson S A, Subbarao K V, Kelley S P and Dickin A P 2003 Early Proterozoic melt generation processes beneath the intra-cratonic Cuddapah Basin, Southern India; *J. Petrol.* **44(12)** 2139–2171.

Anil K, Gopalan K, Rao K R P and Nayak S S 2001 Rb-Sr ages of kimberlites and lamproites from Eastern Dharwar craton, South India; *J. Geol. Soc. India* **58** 135–142.

Chakraborty M and Das S 2016 35th IGC abstracts, 391p.

Chakraborty K, Mukhopadhyay P K and Pankaj P 2016 Magmatism in Western Cuddapahs: The mafic sills and lava flows of Vempalle and Tadpatri formations; *J. Geol. Soc. India* **87** 631–660.

Das S and Chakraborty M 2015 Report on specialized thematic mapping of ultrapotassic volcanic rocks and associated magmatism in Nallamalai Fold Belt of Proterozoic Cuddapah Basin and their bearing on mineralization around Rajampeta area, Cuddapah district, Andhra Pradesh, Geological Survey of India, unpublished progress report.

Das S and Shukla D 2016 Geochemical signatures of Island Arc Tholeiites from the Central-Western part of Nellore Schist belt, Pamuru–Udayagiri area, Andhra Pradesh, India; *Indian J. Geosci.* 247–262.

Dharma Rao C V and .Reddy U V B 2009 Petrological and geochemical characterization of Proterozoic ophiolitic mélange, Nellore–Khammam schist belt, SE India; *J. Asian Earth Sci.* **36(4–5)** 261–276.

Dobmeier C J and Raith M M 2003 Crustal architecture and evolution of the Eastern Ghat belts of adjacent regions of India; In: Proterozoic East Gondwana: Super continent assembly and breakup (eds) Yoshida M, Windley B F and Dasgupta S, *Geol. Soc. London, Spec. Publ.* **206** 145–168.

ERSOY EmrahYalçın PETROMODELER (Petrological Modeler) 2013 A Microsoft® Excel© spreadsheet program for modelling melting, mixing, crystallization and assimilation processes in magmatic systems; *Turkish J. Earth Sci.* **22** 115–125.

Feigenson M D, Lina C P and Michael J C 1996 Constrains on partial melting imposed by rare earth element variations in Mauna Kea basalt; *J. Geophys. Res.* **101(5)** 11815–11829.

French J E, Heamana L M, Chacko T H and Srivastava R K 2008 1891–1883 Ma Southern Bastar–Cuddapah mafic igneous events, India: A newly recognized large igneous province; *Precamb. Res.* **160** 308–322.

Goodenough K M, Upton B G J and Ellam R M 2002 Long-term memory of subduction processes in the lithospheric mantle: Evidence from the geochemistry of basic dykes in the Gardar Province of South Greenland; *J. Geol. Soc. London*, pp. **159** 705–714.

Halls H C 1982 The importance and potential of Mafic dyke swarms in studies of geodynamic processes; *Geol. Assoc. Canada*, pp. 145–154.

Irvine T N and Baragar W R A 1971 A guide to the chemical classification of the common volcanic rocks; *Can. J. Earth Sci.* **8** 523–548.

Jensen L S 1976 *A new cation plot for classifying subalkalic volcanic rocks*; Ontario Div. Mines, Misc. Paper 66.

Khanna T C 2013 Geochemical evidence for a paired arc–back-arc association in the Neo-Archaean Gadwal greenstone belt, Eastern Dharwar Craton, India; *Curr. Sci.* **104(5)** 632–640.

King W 1872 On the Kadapah and Kurnool formations in the Madras Presidency; *Mem. Geo. Surv. India* **8(1)** 346p.

Kostopoulos D K 1991 Melting of the shallow upper mantle: A new perspective; *J. Petrol.* **32(4)** 671–699.

Lindsley D H 1983 Pyroxene thermometry; *Am. Mineral.* **68** 477–493.

Manikyambaa C, Ganguly S, Santosh M, Saha A, Chatterjee A C and Khelena A 2015 Neoarchean arc–juvenile back-arc magmatism in eastern Dharwar Craton, India: Geochemical fingerprints from the basalts of Kadiri greenstone belt; *Precamb. Res.* **258** 1–23.

Meschede M 1986 A method of discriminating between different types of mid-ocean ridge basalts and continental tholeiites with the Nb–Zr–Y diagram; *Chem. Geol.* **56** 207–218.

Miyashiro A 1974 Volcanic rock series in island arcs and active continental margins; *Am. J. Sci.* **274** 321–355.

Nagaraja Rao B K, Rajurkar S T, Ramalingaswamy G and Ravindra B 1987 Stratigraphy and structure and evolution of the Cuddapah basin; *J. Geol. Soc. India Mem.* **06** 33–86.

Narayana Rao M 1983 Lithostratigraphy of the Precambrian rocks of the Nellore Schist Belt; *Quart. J. Geol. Min. Metall. Soc. India* **55** 83–89.

Palme H and O'Neill H St C 2014 Cosmochemical estimates of Mantle composition; In: *Treatise on geochemistry* (eds) Holland H D and Turrekian K K, Elsevier, Amsterdam, The Netherlands **2** 1–38.

Pearce J A 1982 Trace element characteristics of lavas from destructive plate boundaries; In: *Andesites: Orogenic*

Andesites and related rocks (ed.) Thorpe R S, John Wiley & Sons, Chichester, pp. 525–548.

Pearce J A 1983 Role of the sub-continental lithosphere in magma genesis at active continental margins; In: *Continental basalts and mantle xenoliths* (eds) Hawkesworth C J and Norry M J, Shiva, Orpington (London), and Birkhauser Boston, Cambridge, MA, pp. 230–249.

Pearce J A and Cann J R 1973 Tectonic setting of basic volcanic rocks determined using trace element analyses; *Earth Planet. Sci. Lett.* **19** 290–300.

Rajamani V, Shirey S B and Flanson G N 1989 Fe rich Archean tholeiites derived from melt enriched mantle sources: Evidence from the Kolarschist belt, south India; *J. Geol.* **97** 487–501.

Ramam P K and Murty V N 1997 Geology of Andhra Pradesh, Geological Society of India, Bangalore, 245p.

Rao C N V 2007 Chelima Dykes, Cuddapah Basin, Southern India: A review of the age, petrology, geochemistry and petro genesis of world's oldest lamproites; *J. Geol. Soc. India* **69** 523–538.

Rao C N V, Gibson S A, Pyle D M and Dickin A P 2004 Petrogenesis of Proterozoic lamproites and kimberlites from the Cuddapah Basin and Dharwar Craton, Southern India; *J. Petrol.* **45** 907–948.

Rao C N V, Yuan W F and Srinivas M 2012 Mesoproterozoic emplacement and enriched mantle derivation of the Racherla alkali syenite, Palaeo-Mesoproterozoic Cuddapah Basin, southern India: Insights from in situ Sr-Nd isotopic analysis on Apatite; *Geol. Soc. London, Spec. Publ.* **365** 185–195.

Ravikant V 2010 Palaeoproterozoic (1.9 Ga) extension and breakup along the eastern margin of the Eastern Dharwar Craton, SE India: New Sm–Nd isochron age constraints from anorogenic mafic magmatism in the Neoarchean Nellore greenstone belt; *J. Asian Earth Sci.* **12** 67–81.

Saha D and Sain A 2018 Multiple convergences along an Archean craton margin: Clues from Proterozoic ophiolite remnants, granites and granulite domains along the SE margin of India.

Saha D and Tripathy V 2012 Palaeoproterozoic sedimentation in the Cuddapah Basin, south India and regional tectonics. A review; *Geol. Soc. London* **365** 161–184.

Schweitzer J and Kröner A 1985 Geochemistry and petrogenesis of early Proterozoic intracratonic volcanic rocks of the Ventersdrop Supergroup, South Africa; *Chem. Geol.* **51** 265–288.

Sesha Sai V V 2011 Petrology and mineral chemistry of picrite sill from Peddakudala-Velpula area, in Southwestern part of the Proterozoic Cuddapah Basin, Andhra Pradesh, India; In: *Dyke swarms: Keys for geodynamic interpretation* (eds) Srivastava R K, Springer Verlag, Germany.

Sesha Sai V V 2014 Pyroclastic Volcanism in Papaghni Sub-basin, Andhra Pradesh: Significant Paleoproterozoic Tectonomagmatic event in SW part of the Cuddapah Basin, Eastern Dharwar Craton; *J. Geol. Soc. India* **83** 355–362.

Sharkov E, Bogina M and Chistyakov A 2016 Magmatic systems of large continental igneous provinces; *Geosci. Front.* **XXX** 1–20.

Shaw D M 2007 *Trace elements and magma – A theoretical treatment* (ed.) Taylor S R, Cambridge University Press, New York, USA.

Sheppard S, Rasmussen B, Jian-Wei Zi, Soma Sekhar V, Srinivasa Sarma D, Ram Mohan M, Krapež B, Wilde S A and McNaughton N J 2017 U–Pb dating of metamorphic monazite establishes a Pan-African age for tectonism in the Nallamalai Fold Belt, India; *J. Geol. Soc.* **174** 1062–1069.

Srivastava R K (ed.) 2011 *Dyke swarms: Keys for geodynamic interpretation*. Springer-Verlag, Berlin, Germany.

Srivastava R K 2012 Early Precambrian mafic dyke swarms from the Central Archaean Bastar Craton, India: Geochemistry, petrogenesis and tectonic implications; *Geol. J.* **47** 144–160.

Srivastava R K and Singh R K 2004 Trace element geochemistry and genesis of Precambrian sub-alkaline mafic dykes from the central Indian craton: Evidence for mantle metasomatism; *J. Asian Earth Sci.* **23** 373–389.

Srivastava R K, Jayananda M, Gautam C G and Samal A K 2014 Geochemical studies and petrogenesis of $\sim$ 2.21–2.22 GaKunigal mafic dyke swarm (trending N–S to NNW–SSE) from eastern Dharwar craton, India: Implications for Paleoproterozoic large igneous provinces and supercratonsuperia; *Mineral. Petrol.* **108(5)** 695–711.

Sun S and McDonough W F 1989 Chemical and isotopic systematics of oceanic basalts implications for mantle composition and processes; *Geol. Soc. London, Spec. Publ.* **42** 313–345.

Vasudevan D and Rao T M 1975 The high grade schistose rocks of Nellore Schist Belt, Andhra Pradesh and their geologic evolution; *Ind. Mineral.* **16** 43–47.

Verma S P and Gómez M A R 2013 New computer program TecD for tectonomagmatic discrimination from discriminant function diagrams for basic and ultrabasic magmas and its application to ancient rocks; *J. Iberian Geol.* **39(1)** 167–179.

Verma S P and Verma S K 2013 First 15 probability-based multidimensional tectonic discrimination diagrams for intermediate magmas and their robustness against post-emplacement compositional changes and petrogenetic processes; *Turkish J. Earth Sci.* **22** 931–995.

Vijaya Kumar K, Narsimha Reddy M and Leelanandam C 2006 Dynamic melting of the Precambrian mantle: Evidence from rare earth elements of the amphibolites from the Nellore–Khammam Schist Belt, south India; *Contrib. Mineral. Petrol.* **152** 243–256.

Winchester J A and Floyd P A 1977 Geochemical discrimination of different magma series and their products using immobile elements; *Chem. Geol.* **20** 325–343.

Corresponding editor: Rajneesh Bhutani